Electrochimica Acta 247 (2017) 674–684

Contents lists available at ScienceDirect

Electrochimica Acta

journal homepage: www.elsevier.com/locate/electacta

High surface area Pd nanocatalyst on core-shell tungsten based support as a beneficial catalyst for low temperature fuel cells application

N.R. Elezovic[a,*,1], P. Zabinski[b], P. Ercius[c], M. Wytrwal[e], V.R. Radmilovic[d], U.Č. Lačnjevac[a], N.V. Krstajic[d]

[a] Institute for Multidisciplinary Research, University of Belgrade, Kneza Viseslava 1, 11030 Belgrade, Serbia
[b] AGH University of Science and Technology, Faculty of Non-Ferrous Metals, Al. Mickiewicza 30, 30-059 Krakow, Poland
[c] National Center for Electron Microscopy, LBNL University of California, Berkeley, CA, USA
[d] Faculty of Technology and Metallurgy University of Belgrade, Karnegijeva 4, 11000 Belgrade, Serbia
[e] AGH University of Science and Technology, Academic Centre for Materials and Nanotechnology, Al. Mickiewicza 30,30-059 Krakow, Poland

ARTICLE INFO

Article history:
Received 25 April 2017
Received in revised form 7 July 2017
Accepted 10 July 2017
Available online 12 July 2017

Keywords:
fuel cells
oxygen reduction
Pd nanoparticles
tungsten based support
core-shell structure

ABSTRACT

Tungsten based support was prepared by polycondensation of resorcinol and formaldehyde from ammonium metatungstate, in the presence cetyltrimethylammonium bromide (CTABr) surfactant. Pd nanocatalyst on this support was synthesized by borohydride reduction method. The obtained materials were characterized by High Resolution Transmission Electron Microscopy (HRTEM), Electron Energy Loss Spectroscopy (EELS), X-ray Photoelectron Spectroscopy (XPS) and electrochemical measurements. TEM analysis revealed Pd nanoparticles size in the range of a few nanometers, even the clusters of single Pd atoms. X-Ray Photoelectron Spectroscopy was applied to determine surface composition of the substrates. It was found that tungsten based support consisted of W, WC and WO_3 species. The presence of metallic palladium – Pd(0) in the Pd/W@WCWO_3 catalyst was revealed, as well. The catalytic activity and stability for the oxygen reduction were investigated in acid and alkaline solutions, by cyclic voltammetry and linear sweep voltammetry at the rotating disc electrode. The catalysts' activities were compared to the carbon supported Pd nanoparticles (Vulcan XC 72). WC supported Pd nanoparticles have shown high activity and superior stability, comparable even to Pt based catalysts, especially in alkaline electrolytes.

1. Introduction

Low temperature fuel cells are promising environmental friendly future power sources. The main advantages are: high conversion efficiency, variety of fuels used (hydrogen, low molecular alcohols . . .) using cheap available oxygen from air as oxidative agent, small number of mobile device parts, silent working conditions. For polymer electrolyte membrane fuel cells platinum and platinum alloys nanocatalysts onto carbon based supports are state of the art materials for practical application [1–6]. However, due to the high price and scarcity of Pt the large commercialization is prevented so far. Although carbon based materials possess many desirable properties, such as high surface area, high conductivity, relatively low cost and easy synthesis, the large scale commercialization is limited by insufficient stability, especially at high positive potential values (1.4 V vs RHE and higher) [7]. Degradation of the fuel cells catalyst during exposure to high anodic potentials, especially at the startup/shut down conditions, has been already emphasized in literature, causing insufficient catalysts' durability, even the whole fuel cell degradation during the long time use [8–10]. Development of high activity and stability nanostructured catalysts for fuel cells reactions is very important, especially for oxygen reduction, as its high overpotential and slow kinetics prevents wide commercialization, as well. It is well known that the performance of fuel cell is much more influenced by oxygen reduction kinetics, if compared to fast hydrogen oxidation. Namely, the thermodynamic reversible potential for oxygen reduction reaction in water solutions is 1.23 V vs RHE, while the established open circuit potential is about 0.3 V lower. This large potential loss is attributed to the surface coverage with oxygen containing species from water (e.g. OH), or other adsorbed anions. Thus, further improvement of fuel cell performance implies development of a more active catalyst for

* Corresponding author.
E-mail address: elezovic@imsi.rs (N.R. Elezovic).
[1] ECS and ISE member.

http://dx.doi.org/10.1016/j.electacta.2017.07.066
0013-4686/

oxygen reduction. The importance of synthesis and processing of nanostructured catalysts with controlled size, composition, and surface properties for electrocatalytic oxygen reduction was emphasized [6].

Palladium is considered as the most Pt-like metal, and second most active noble metal for oxygen reduction, but its electrocatalytic activity for ORR appears to be much lower than that of Pt. The electrocatalytic performance and durability of Pd based nano-catalysts can be further improved by using novel carbon materials as supports or metal oxides as catalyst promoters [11]. For instance, highly reduced graphene oxide HRG/Pd–MWCNT nano composites have shown enhanced ORR activity and excellent durability [12].

Well-ordered and homogeneous Pd cubic-shaped nanoparticles with and without a support, synthesized through an aqueous chemical synthesis with an average nanoparticle size of 17.5 and 10.6 nm, have shown a much better performance in the oxygen reduction reaction than commercial Pd [13]. Recent investigations have validated that the ORR activity of Pd can be effectively enhanced by alloying with other elements. The as-prepared PdAu alloys displayed improved catalytic activities and better stabilities for oxygen reduction reaction (ORR) compared to commercial E-TEK Pt/C, Pt black and Pd black [14].

Palladium based nanocatalysts have been recently introduced as adequate substitute for Pt as the catalysts towards oxygen reduction, owing much lower price than Pt, as well as relatively high activity, especially in alkaline solutions [15–18]. Improvements in the activity of palladium have been achieved by alloying nanostructured palladium with other transition metals. It is considered that the incorporation of Ni with Pd could cause favorable change of Pd electron structure to modify the reaction kinetics for ORR on NP-PdNi alloys, thus resulting in high ORR performance [19].

Palladium supported on thermally treated carbon (Pd/TTC) synthesized by $NaBH_4$ reduction, showed high activity for oxygen reduction, following kinetics of four electrons transfer. This behavior was attributed to structural properties and superficial conditions of the supporting carbon [20]. L. Jiang et al. discussed the challenges for using Pd/C as an ORR catalyst in alkaline solutions and showed high activity toward the oxygen reduction reaction both at room and elevated temperatures (up to 60 °C), if compared with the Pt/C [21]. A carbon-supported palladium catalyst modified by non-metal phosphorus (PdP/C) has been recently developed and tested as an oxygen reduction catalyst, showing activity comparable to the commercial Pt/C catalyst and a higher than the Pd/C catalyst synthesized by the conventional $NaBH_4$ reduction method [22]. Its high catalytic activity was attributed to lower relative crystallinity, and the formation of PdP alloy [22]. Tailoring the conditions of electrochemical synthesis to obtain Pd based catalysts from nanoparticles to nanorods, it was found a strong dependence of the activity of Pd towards the ORR on its morphology [23]. The morphology of Pd-nanorods featured the exposure of Pd(110) facets, exhibiting superior ORR activity. The mechanism, indicated by DFT calculations, was ascribed to the exceptionally weak interaction between an O adatom and a Pd(110) facet [23]. The Oxygen reduction rate for Pd based catalysts seems to depend strongly on the orientations of the Pd surface with Pd (100) having a much higher ORR activity than any other facet in acid electrolytes [24]. As for long term stability, future research may focus on improving the durability of Pd-based catalysts by surface modification and/or composition optimization [24].

Pd@Pt/CNT bimetallic or core@shell catalysts was developed by Xia et al. The excellent catalytic activity of the Pd@Pt/CNT was ascribed to the synergistic function of Pt and Pd towards the ORR [25].

Palladium and platinum have very similar properties because they belong to the same group in the periodic table. The activity for the oxygen reduction reaction (ORR) of Pd can be only slightly lower than that of Pt, and by addition of a suitable metal, such as Co or Fe, the ORR activity of Pd can even overcome that of Pt [26]. Carrera-Cerritos et al. investigated reduced graphene oxide (rGO) as a support for Pt and Pd. Pd nano-catalyst showed an enhanced performance when is supported on rGO [27]. Palladium catalysts supported on titanium suboxides (Pd/Ti_nO_{2n-1}) were prepared by the sulphite complex route [28]. Pd/Ti_nO2_{n-1} catalyst showed a very promising stability compared to carbon-supported Pd samples in an accelerated degradation test of 1000 potential cycles. These results indicated good perspectives for the application of Pd/Ti_nO_{2n-1} catalysts in DMFC cathodes [28].

In this manuscript high surface area novel Pd nanocatalyst onto core shell type structure tungsten based support was synthesized and characterized for oxygen reduction, in both acid and alkaline solutions. The catalytic activity and stability of the catalyst were tested and compared to carbon supported Pd nanoparticles.

2. Experimental

Core-shell tungsten based support was synthesized by modified Ganesan and Lee procedure [29]. Tungsten based support assigned as $W@WCWO_3$ was prepared from ammonium metatungstate by polycondensation of resorcinol and formaldehyde in the presence of cetyltrimethylammoniumbromide (CTABr) surfactant. 6.14 g CTABr was dissolved in 20 ml of 18 MΩ distilled water. The solution containing 4.073 g of ammonium metatungstate salt, 1.13 g of resorcinol and 1.7 ml of formaldehyde in 10 ml H2O was added to the CTABr surfactant solution. Solution was decanted, sealed and placed for 3 days at 25oC, 1 day at 55 °C and 3 days at 85 °C. Resorcinol/formaldehyde gel was immersed in a 10-times volume of 2-Methyl-2-propanol for one day. After that time, rinsing with 2-Methyl-2-propanol was repeated twice.

The sample was pre-frozen at −30oC for 24 h. Then it was exposed to freeze drying procedure for twenty four hours at the pressure of 4 mbar. The red colored gel was treated in furnace with argon atmosphere, at 950 °C for 1 h. Pd(10%) nanoparticles were deposited onto it by borohydride reduction method. Pd(10%)XC catalyst, used as benchmark, was synthesized by borohydride reduction, onto commercial carbon support, Vulcan XC 72, E-TEK.

2.1. X-ray diffraction

The support material was characterized by X-ray diffraction (XRD) technique on a Siemens D500 X-ray diffractometer using CuK radiation with a Ni filter. The scan rate applied was 0.02∘/s.

2.2. HRTEM characterization

The samples were characterized for morphology, particle size distribution and chemical composition by high angle annular dark filed scanning transmission electron microscopy (HAADF, STEM) using aberration corrected TEAM0.5 transmission electron microscope operated at 80 kV and 300 kV. HAADF was chosen because of its strong correlation between atomic number and image intensity, enabling it easy to distinguish between heavy and light elements particles. In order to take into account the non-spherical shape, major and minor axes of all particles were measured, from which average particle diameters were extracted. A point energy dispersive spectroscopy (EDS) was performed on the CM200-FEG transmission electron microscope operated at 200 kV in the STEM mode using 1 nm beam size. High resolution phase contrast imaging (HREM) was performed by the Titan 80–300 kV non-corrected transmission electron microscope. Crystallographic information from individual Pd particles, such as the presence of facets, equilibrium shape, etc., was obtained by numerical

Fourier filtering (FFT, Fast Fourier Transformation) of the digital image intensity spectra.

Particle size distribution was determined from TEM images based on average 20 different regions of the catalyst; each region contained from 10 to 20 particles. The particle shapes were determined by real space crystallography with the use of high-resolution images taken from particles near or on the edge of the substrate, and/or by numerical Fourier filtering of the digitized image intensity spectrum of particles on top of the support.

All TEM characterization was done at the National Center for Electron Microscopy, Lawrence Berkeley National Laboratory.

2.3. XPS surface characterization

X-ray photoelectron spectroscopy measurements were performed using a PHI 5000 Versa Probe II (ULVAC-PHI, Chigasaki, Japan) spectrometer equipped with an Al Kα radiation source (1486.6 eV). A photoelectron take-off angle Θ equal to 45° was applied for the measurements. A dual-beam charge neutralizer was used to compensate the charge-up effect. High resolution spectra were recorded with analyzer pass energy of 29.35 eV. The operating pressure in the analytical chamber was less than 5×10^{-7} Pa. XPS spectra were acquired from $400 \times 300\ \mu m^2$ areas. All XPS peaks were charge referenced to the neutral (C—C) carbon C 1s peak at 284.8 eV. The spectrum background was subtracted using the Shirley method. Data analysis software from PHI MultiPak was used to calculate elemental compositions from the peak areas.

2.4. Electrochemical characterization

Electrochemical experiments were done in a standard three compartment electrochemical cell. Pt foil of the surface area of $5\ cm^2$ was applied as a counter electrode, while reversible hydrogen electrode was used as a reference. Rotating disc electrode experiments were done at gold rotating disc electrode, of 5 mm diameter. Cyclic voltammetry experiments were done in nitrogen purged 0.1 mol dm^{-3} NaOH and 0.5 mol $dm^{-3}HClO_4$ respectively, with the sweep rate of 100 mV s^{-1}. Polarization curves were recorded in O_2 saturated 0.1 mol dm^{-3} NaOH and 0.5 mol $dm^{-3}HClO_4$, respectively, at the different rotation rates and sweep rate of 20 mV s^{-1}. Prior to the experiments the rotating disc electrode was polished by 0.5 μm alumina powders and rinsed in 18 MΩ water. After that an aliquot of catalyst ink was transferred by micropipette and dried during 15 minutes at 80°C, to enable Nafion polymerization. The catalyst loading was kept constant – 40 μg cm^{-2} Pd, expressed per geometric electrode surface area.

Stability tests were performed by repetitive cycling in the potential range from 0 V to 1.4 V vs RHE, at the sweep rate of 100 mV s^{-1}. Prior to the cycling and after that the polarization curves for oxygen reduction were recorded, applying positive going sweep at a sweep rate of 20 mV s^{-1}, to compare the activities. This is well known durability testing procedure, for testing the durability of a support material approved by US Department of Energy.

3. RESULTS AND DISCUSSION

3.1. HRTEM results for the catalyst and support

HRTEM images for the tungsten based support are presented in Fig. 1a and b. Quite homogeneous particle size distribution is proven (Fig. 1a). Core shell type structure, containing W core and shell made of tungsten based oxide and carbide is shown in Fig. 1b.

Han et al. demonstrated that core–shell nanostructures can strongly influence catalyst's stability, improving base metal retention and leading to exceptional durability [30]. Core shell structure was proven by Electron Energy Loss Spectroscopy, as well. Single EELS spectra recorded from support particle, as well as EDS analysis of support shell were presented in ESI (Fig. S1, Fig.S2, respectively). Namely, in Fig.S1 single EELS spectra of WC simultaneously performed with High Angle Annular Dark Field transmission electron microscopy, showing the thickness of WC island on W particle ~1 nm, in this specific case. Line scan was performed across edge of W particle and WC island. Dotted lines indicate the region in HAADF image where EELS CK line is present.

In Fig. S2 HRTEM image showing core shell structure of tungsten based support is presented, as well. Black dot in this image shows the position where the EDS analysis of the shell is performed. This indicates that the shell could be made of tungsten carbide and tungsten oxide, as it would be confirmed by XPS analysis later (written below).

Low magnification TEM image and High angle annular dark field images (HAADF) for Pd nanoparticles onto tungsten based support are presented in Fig. 2a and 2b.

Very small Pd nanoparticle size, even the single atoms clusters can be seen. The average particle size was ca. 2.5 nm, implying that the kinetics of the formation of the seeds were faster than growth. The histogram of particle size distribution was shown in ESI (Fig. S3).

3.2. XPS spectra of $W@WCWO_3$ support and $Pd/W@WCWO_3$ catalyst

X-ray photoelectron spectroscopy (XPS) confirmed the presence of C, O, Pd and W in $Pd/W@WCWO_3$ sample (Fig. 3a) and C, O and W in $W@WCWO_3$ sample (Fig. 3b). The total amount of each element contribution in both samples is presented in Table 1. Detection of carbon in $Pd/W@WCWO_3$ sample could be justified by the presence of organic compounds as residues after sample preparation. It is obvious the presence of carbon 1s spectral line in all samples. It is well known that XPS analyses only several atomic layers on the surface and presence of carbon is usually detected. Namely, the surface contamination by carbon dioxide from air is almost unavoidable, as it was already referred in literature. It is common problem when the samples were exposed to air, even if the sample transfer was done quickly. On the other hand, carbon signal is usually used to calibrate XPS machine for measurements.

The detailed analysis of contribution of bound type in $Pd/W@WCWO_3$ sample is presented in Table 2 and the fitted peaks are shown on Fig. 4. Despite of C-C and C-O bonds as organic and inorganic contaminations, $Pd/W@WCWO_3$ consists mainly of WO_3 and palladium. The W 4f spectrum confirms the presence of pure WO_3 which is clearly defined by the 4 $f_{7/2}$ peak set at 36.0 eV with doublet separation of 2.14 eV (Fig. 4d)[31]. Moreover the presence of oxygen O 1s peak corresponds to WO_3 both, in respect to binding energy – 531.0 eV [28]. (Fig. 4b) and WO_3 atomic ratio (W:O/1:3) (Table 2). The Pd 3d spectrum (Fig. 4c) can be fitted by two doublets with the binding energies of the Pd $3d_{5/2}$ component at 335.7 eV and 337.3 eV, respectively. First peak is attributed to metallic Pd, while the second peak comes from Pd(II) [32,33]. The presence of some amount of Pd(II) besides metallic Pd could be explained by residues from the Pd precursor solution, remained at the surface.

The detailed analysis of contribution of bound type in WC sample is presented in Table 3 and the fitted peaks are shown on Fig. 5. Our analysis confirms the presence of W-C bond in C 1s spectrum at 282.8 eV (Fig. 5a) [34]. Moreover, the presence of carbon organic residues is detected. The O 1s spectrum in Fig. 5b shows two types of oxygen at 530.8 and 532.1 eV, corresponding to W-O and C-O (single and double from the organic residues) bonds, respectively. The W 4f spectrum can be fitted by three doublets with the binding energies of the W $4f_{7/2}$ component at 31.8, 32.5

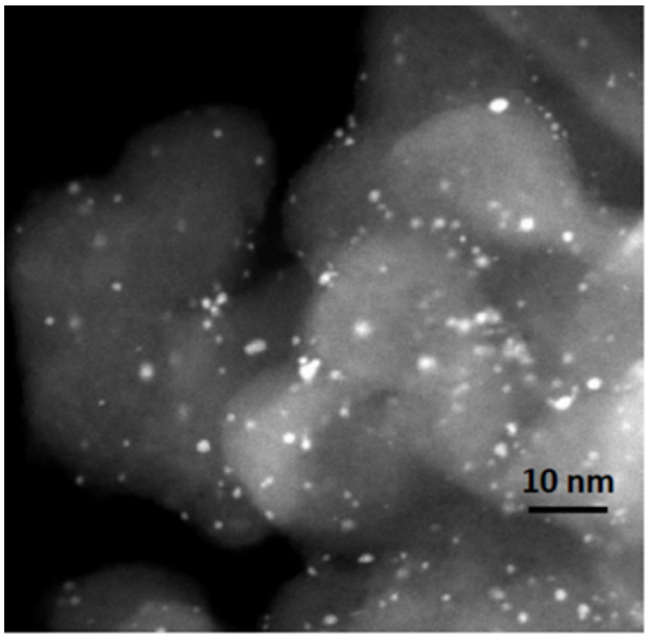

a

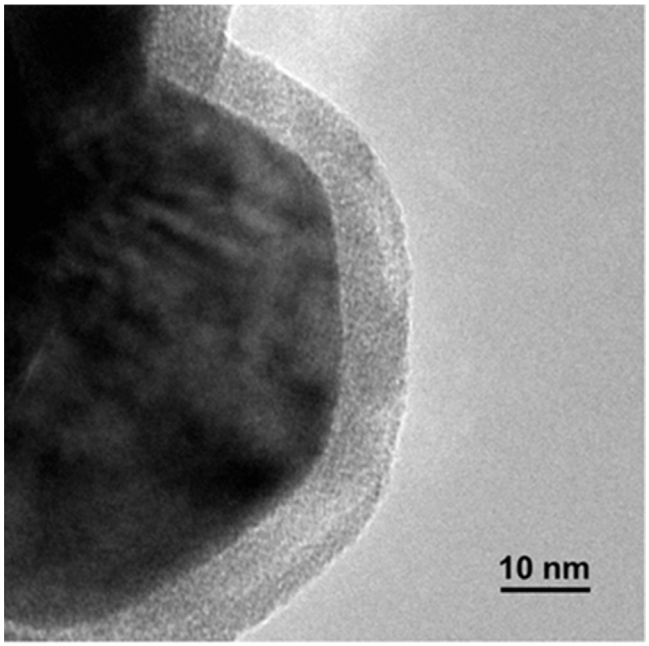

b

Fig. 1. HRTEM images of W@WCWO3 support: a) Smaller W particles (cluster); b) Core-shell structure; EDS analysis indicated that the shell is made of mixture, W-oxide and W-carbide(s) (Fig.S2,ESI).

and 35.9 eV, respectively (Fig. 5c). These are attributed to metallic W, W carbide and WO_3 [35,36].

These results were confirmed by X-ray diffraction, where W and WC species were found (Fig.S4, ESI). As for some discrepancy between XPS and XRD results, it should be emphasized the following facts:

The XRD measurements of as prepared nanoparticles are common complicated, e.g. low crystallinity, quasi amorphous structure is usually obtained. We have annealed the samples at 100 °C in inert atmosphere to obtain better defined grains. It is well known that tungsten oxide could be amorphous up to 300 °C. It could be explanation of different phase composition obtained by XPS and XRD measurements, e.g. absence of tungsten oxide at the X-ray diffractogram of the tungsten based support. On the other hand, by XRD usually bulk composition is determined, while by XPS the composition of several atomic layers on the surface is considered. The surface contamination of only several atomic layers, in a case of XPS measurements could be much more pronounced, as well. Anyway, it is confirmed that the core is made of tungsten, while shell is made of WC and WO_3. The shell thickness is estimated to be from 1 to 5 nm. It has been confirmed by combination of HRTEM, EELS and EDS techniques.

As for XPS and XRD results, it is important to note that there were no W_2C tungsten carbide species, well known as instable in the potential range of interest for oxygen reduction reaction.

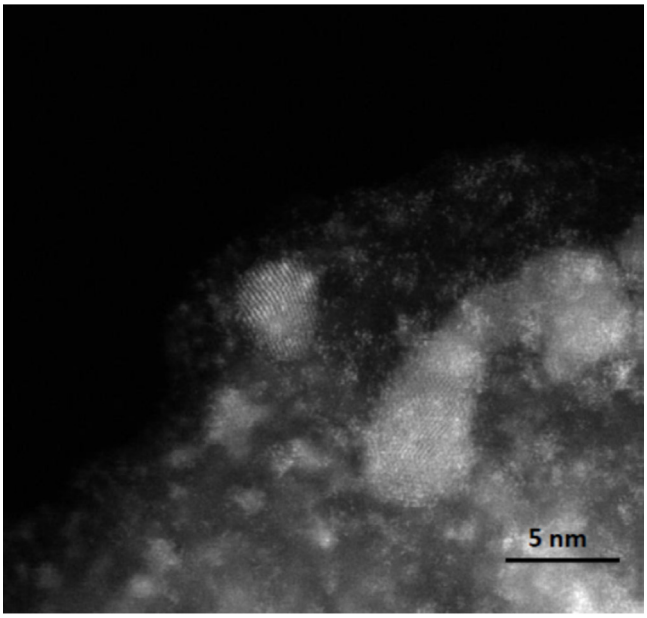

a

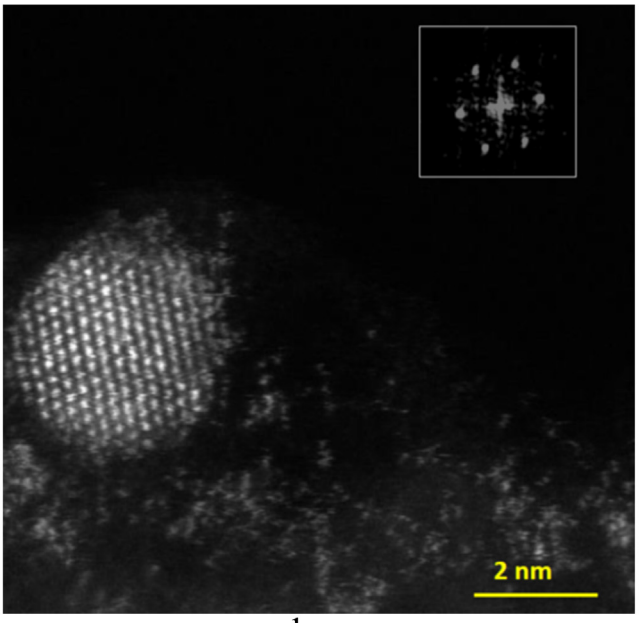

b

Fig. 2. a) HAADF image of Pd clusters and larger particles taken at 300 kV; b)HAADF image of Pd single atoms and clusters taken close to 110 zone axis at 300 kV.

3.3. Electrochemical characterization – oxygen reduction reaction

Cyclic voltammograms of Pd/W@WCWO$_3$ catalyst recorded in N_2 saturated acid electrolyte for different upper potential limits are shown in Fig. 6a. This method is applied for the determination of the real, electrochemically active Pd surface area, as it was already suggested in literature [37]. In order to use the charge for the formation of a full monolayer of PdO for real surface area determination, it implies to determine upper potential limit at which oxygen is chemisorbed in a monoatomic layer with a one-to-one correspondence with the surface Pd atoms [38,39]. In this case the charge associated with the formation or reduction of the chemisorbed oxygen layer is calculated ca. 420 $\mu C\,cm^{-2}$ for Pd [38,39].

Namely, by integration of cathodic parts of these voltammograms, the charge values corresponding to the reduction of oxygen covered Pd electrode (after double layer correction) are obtained. The charge for the reduction of oxygen covered Pd electrode as a function of the upper potential limit is presented in Fig. 6b. According to Ref. 39, the charge value at the point where the straight line changes its slope corresponds to the formation of a full PdO monolayer. At higher anodic potentials further oxidation occurs on the Pd surface, leading to the formation of Pd oxides of higher valence state. In such a way obtained charge value is divided by 420 μC, as it was the charge corresponding to one monolayer of Pd(II) oxide [37–39]. This analysis gave the value of electrochemically active surface area of 145 $m^2\,g^{-1}$. The obtained value is in good accordance to the one calculated on the basis of HRTEM results,

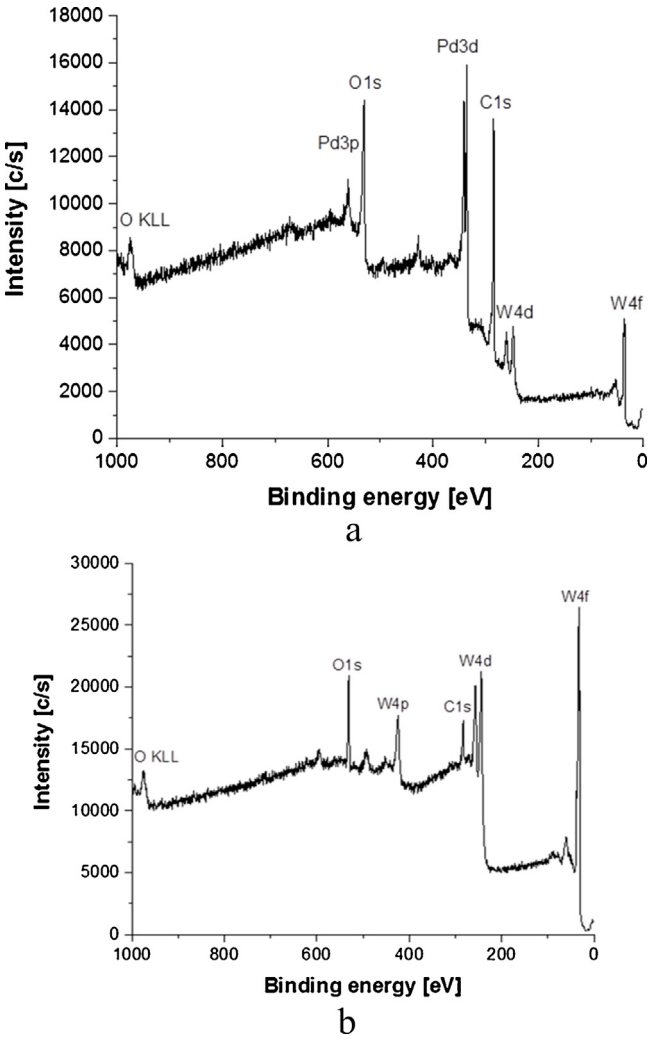

Fig. 3. Survey scan performed with X-ray photoelectron spectroscopy of (a) Pd/W@WCWO$_3$ and (b) W@WCWO$_3$.

Table 1
Total XPS elemental analysis of Pd/W@WCWO$_3$ and W@WCWO$_3$ samples.

Sample	C (%)	O (%)	Pd (%)	W (%)
Pd/W@WCWO3	61.24	29.83	5.80	3.13
W@WCWO3	44.82	27.76	–	27.43

Table 2
The contribution of fitted peaks and bounds type in Pd/W@WCWO$_3$.

C 1s (%)				O 1s (%)		Pd 3d (%)		W 4f (%)
C-C	C-O	C=O	O—C=O	WO_3	C-O, C=O	Pd^0	Pd^{2+}	WO_3
38.56	17.73	2.84	4.00	8.40	19.63	3.84	2.03	2.97

using the average particle size of 2.5 nm. Namely, assuming the spherical symmetry of Pd particles, the specific surface area should be:

$$s = \frac{3}{r \cdot \rho} = \frac{3}{1.25 \cdot 10^{-7} cm \cdot 12.26 g cm^{-3}} = 196 m^2 g^{-1} \quad (1)$$

The above calculated value is about 26% higher than electrochemically determined one, indicating some degree of particle agglomeration, in other words, all particles were not fully accessible for the reaction.

Polarization curves for oxygen reduction, recorded at Pd/W@WCWO$_3$ electrode at the different rotation rates and sweep rate of 20 mV s^{-1}, in acid and alkaline electrolytes, are presented in Fig. S5a and Fig.S5b, Electronic Supplementary Information. It can be seen that the values of onset potentials and half wave potentials of the reaction are more positive in alkaline solution. The presented experimentally obtained values of 0.98 V vs RHE and 0.90 V vs RHE for onset and half wave potential, respectively, are even comparable to platinum based catalysts in the same solution.

The polarization curves for Pd/XC and Pd/W@WCWO$_3$ catalyst, obtained at the same rotation rate of 1625 rpm and sweep rate of 20 mV s^{-1}, in alkaline solution are presented in Fig. 7a. The 30 mV more positive half wave potential is obtained for Pd/W@WCWO$_3$ catalyst. The diffusion limiting current densities are expressed per geometric surface area.

It can be seen that these experimentally obtained diffusion limiting current density values are close to the theoretical ones for the same conditions – electrolyte properties (kinematic viscosity, diffusion coefficient, concentration of dissolved oxygen, at the specific temperature), temperature and rotation rate. Importance of the accordance the experimentally obtained values of diffusion limiting current densities for oxygen reduction with the theoretically calculated for the same conditions was earlier emphasized. It is the indication of the proper, optimally chosen catalyst loading

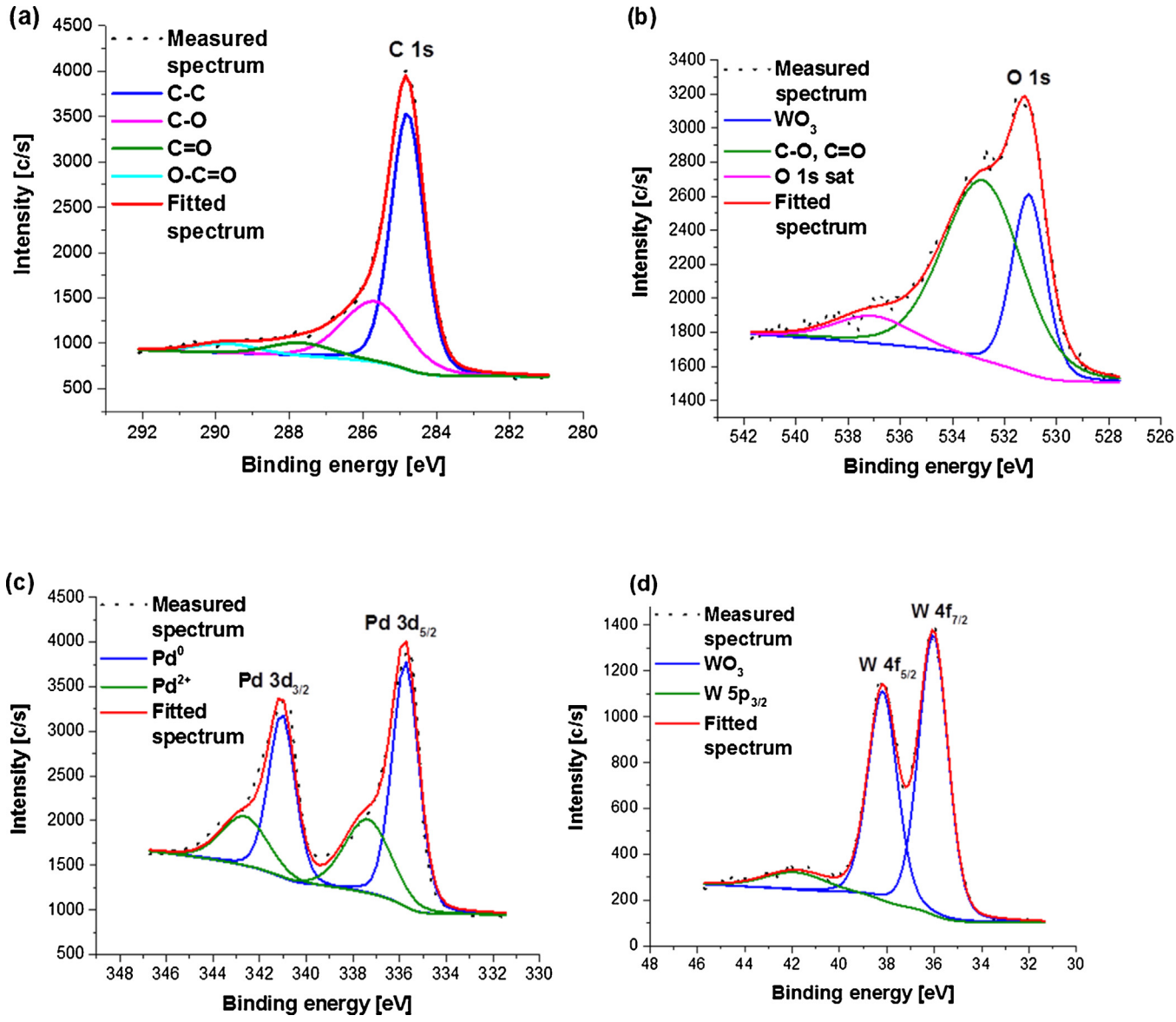

Fig. 4. Elemental analysis of Pd/W@WCWO$_3$ powder: XPS spectra with fitted lines C 1s – (a), O 1s – (b), Pd 3d – (c), W 4f – (d).

Table 3
The contribution of fitted peaks and bounds type in W@WCWO$_3$.

C 1s (%)				O 1s (%)		W 4f (%)		
WC	C-C	C-O	C=O	WO_3	C-O, C=O	W^0	WO_3	WC
15.16	20.50	4.79	3.84	23.82	4.92	10.53	8.00	8.43

[2]. Namely, if the catalyst's loading is too low the rotation disc electrode cannot be completely, homogenously covered, however too high loading value can lead that the mass transport conditions, necessary for rotating disc electrode describing equations, are no longer fulfilled [2].

As the oxygen reduction belongs to mixed control electrochemical reactions, the measured current density is usually presented by Levich-Koutecky equation:

$$\frac{1}{j} = \frac{1}{j_k} + \frac{1}{j_L} \qquad (2)$$

Where: j_k is activation controlled (kinetic) current density and $j_L = B\omega^{1/2}$ is diffusion-limited current density that is a linear function of the square root of the rotation rate. In order to compare catalytic activities in terms of kinetic current densities (per electrochemically active surface area) at the constant potential, the Tafel plots have been presented in Fig. 7b.

Kinetic currents for Tafel plots were determined from equation (2). Two different Tafel slopes are obtained, one ca. 60 mV dec^{-1} and other ca. 120 mV dec^{-1}, in the potential region of low current densities and high currents densities, respectively. These values are in good accordance to already widely accepted literature slope values for oxygen reduction reaction at Pd based catalysts in the same solution. The change of Tafel slope is assigned to the changes of adsorption conditions for adsorbed oxygen containing species, from Temkin to Langmuir type, without changing the rate determining step [40].

It is obvious that almost the same catalytic activities were obtained, expressed in terms of kinetic current densities, per electrochemically active surface area. It is important to note that the value of kinetic current density for Pd/W@WCWO$_3$ catalysts at 0.85 V vs RHE (0.194 mA cm^{-2}) is comparable to widely accepted

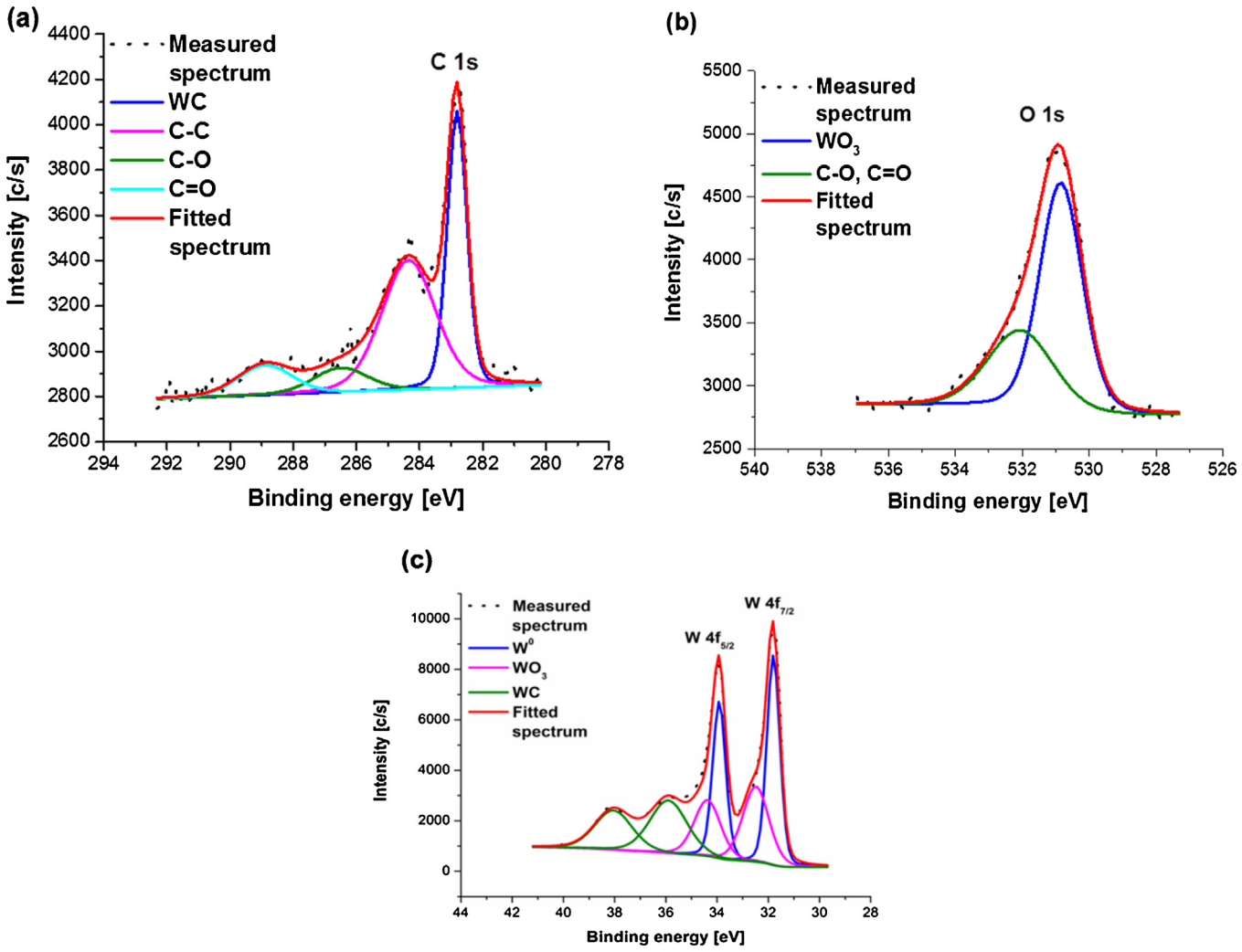

Fig. 5. Elemental analysis of W@WCWO$_3$ powder: XPS spectra with fitted lines C 1s – (a), O 1s – (b), W 4f – (c).

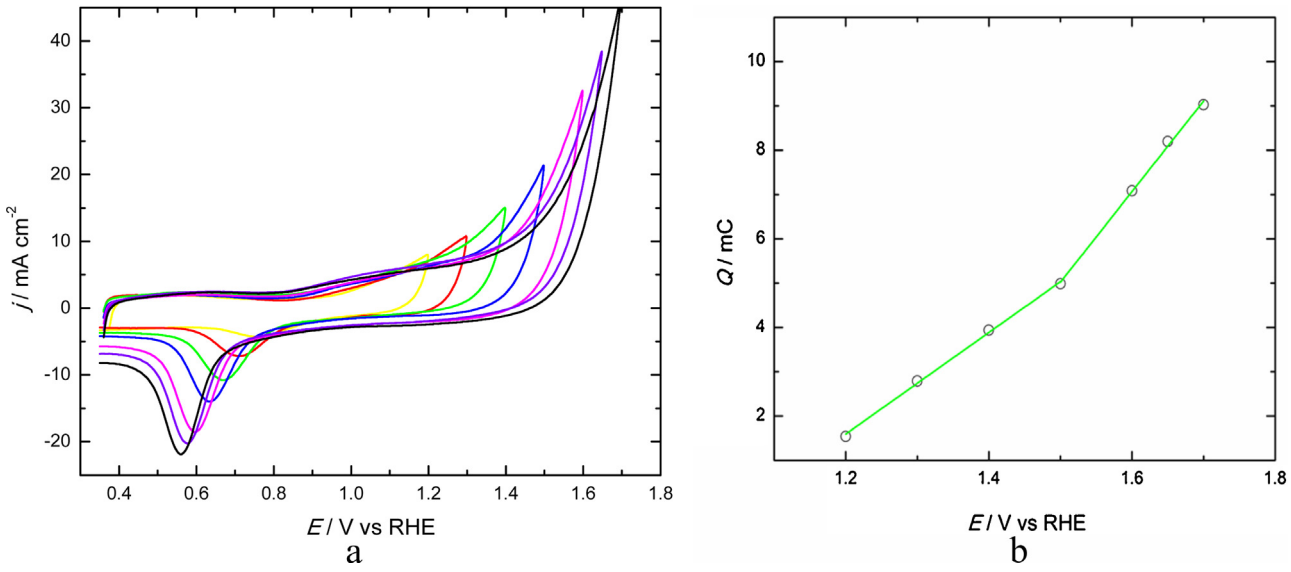

Fig. 6. a) Cyclic voltammograms for Pd/W@WCWO$_3$ catalysts for different upper potential limits, sweep rate 100 mV s^{-1}, N_2 saturated 0.5 mol dm^{-3} $HClO_4$; b) The integrated charge for the reduction of oxygen species covered Pd/W@WCWO$_3$ electrode as a function of the upper potential limit.

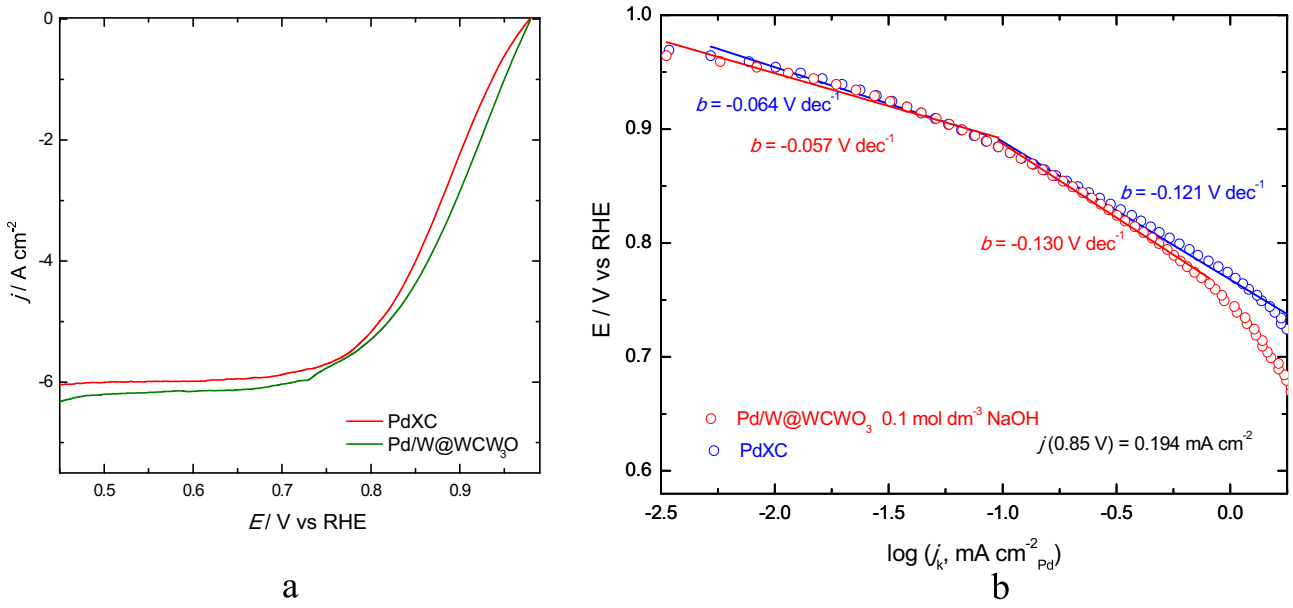

Fig. 7. a)Polarization curves for Pd/XC and Pd/W@WCWO$_3$ catalysts at the same rotation rate, sweep rate 20 mV s^{-1}, in 0.1 mol dm^{-3}NaOH; b) Tafel plost for Pd/XC and Pd/W@WCWO$_3$ catalysts in 0.1 mol dm^{-3} NaOH, at 25 °C.

benchmarks for Pt based catalyst, referred by Gasteiger et al. [41]. Having in mind the strong susceptibility of ORR towards the particles' size and the optimum value around 3 nm for the specific kinetic activity, high kinetic parameters should be expected [42]. The comparison of the electrochemically active surface area values, catalytic activities and half wave potentials, of the relevant literature Pd based catalysts and this one was presented in Table S1, Electronic Supplementary Information. It can be seen that the half wave potential is more positive than any other literature value for Pd based catalysts and electrochemically active surface area is much higher, as well. Very high value of the electrochemically active surface area is caused by homogeneously distributed small particle size, enabling high utilization of the noble metal.

The main problem of contemporary used catalysts for oxygen reduction is insufficient durability, causing catalysts degradation during long time use. Namely, during the startup/shut down procedure the high anodic potential value can be created (1.4 V vs RHE or even more positive), causing corrosion and chemical instability of the catalyst, especially carbon based supports [7–10]. Therefore, the adequate stability is crucial for long life time of the fuel cell. In Fig. 8a and Fig. 8b the results of stability tests for the Pd/W@WCWO$_3$ catalyst in acid and alkaline electrolyte are presented. It can be seen that Pd/W@WCWO$_3$ catalyst exhibited very high stability in alkaline solution. The stability testing results for carbon supported Pd nanocatalyst, showing the support degradation during the repetitive cycling, was presented in ESI, Fig. S6. Namely, after repetitive cycling stability testing performed, the polarization curve for oxygen reduction of Pd/W@WCWO$_3$ is almost the same, like one recorded after the testing procedure (Fig. 8b). It means that there is no support degradation, even at high anodic

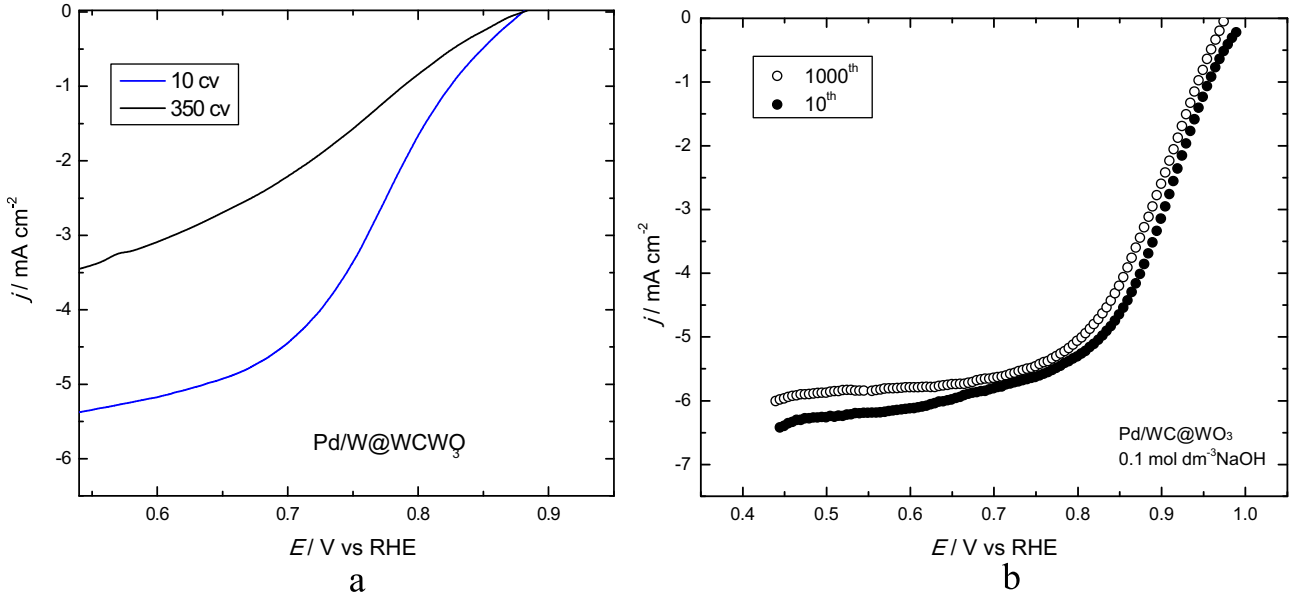

Fig. 8. Polarization curves of Pd/W@WCWO$_3$ catalyst before and after repetitive cycling in the potential range from 0 to 1.4 V vs RHE, sweep rate 20 mV s^{-1}, rotation rate 1600 rpm, in acid (a) and alkaline solution (b).

potentials. These results make the catalyst promising for cathode, having in mind that alkaline anion-exchange membranes (AAEMs) are being developed [43]. As for the stability testing in acid solution (Fig. 8a) it has been stopped after 350th cycle since severe catalyst degradation started, so any further cycling would be meaningless. It is likely that under acidic conditions the tungsten core was selectively etched rather than the surface oxide layer. There are many papers dealing with the stability of the W based species, carbides and oxides, in acidic and alkaline solutions [44,45]. Instability of some tungsten carbide species in acid environment is undoubtedly shown. However, it is also possible that high positive potential value (1.4 V vs RHE) is enough to cause Pd species dissolution in strong acid environment. This possibility has been investigated in early works of Rand and Woods [46].

Additionally, to explain the origin of great properties of Pd/W@WCWO$_3$ catalyst for oxygen reduction, the earlier theoretical consideration, based on the optimization of the ORR rate by tuning the binding energies of the ORR intermediates on the catalyst surface should be mentioned [47]. Namely, the free energy diagrams of ORR reaction on Pd/Fe/W (110), at U = 0.85 V based on DFT calculations, have revealed that the proposed materials can be more active toward ORR than Pt (111) [47]. Thus, the constituting species are expected to couple synergistically yielding reaction-environment stability, cost-effectiveness, and tunable reactivity [47]. The above theoretical consideration is mainly related to acid electrolyte, while for oxygen reduction in alkaline solutions different computational approach has been applied [49]. According to Quaino et al. [49] the rate of the reactions after the transfer of the first electron is the reason for high ORR activity in alkaline solutions. The concentration of the superoxide ion must be very small to shift the O_2/O_2^- equilibrium potential closer to the equilibrium potential for the entire oxygen reduction reaction. These follow-up reactions will also determine if the reaction proceeds by the four-electron path leading to OH^-, or if it stops at peroxide [49].

At the end, the possible role of carbon and its influence on the catalytic activity for oxygen reduction should be elucidated, since some amount of carbon was detected by XPS in all samples. It is well known that at a carbon substrate the oxygen reduction takes place, as well. However it is two electron exchange electrochemical reaction with much lower onset and half wave potential values than any noble metal based catalyst. Tungsten carbide behavior in oxygen reduction is similar, as well. For instance the onset potential of the oxygen reduction reaction on WC is shifted to the negative potentials for about 150 mV. So, the values of oxygen reduction current for WC or carbon itself, in the potential region of practical importance (about 0.85 V vs RHE) are negligible in comparison with the same obtained for noble metal supported nanocatalysts [48]. Therefore, the contribution of the support to the whole current value at the specific potential in the potential region where the ORR takes place on Pd based catalysts (and majority of noble metals, as well) is negligible.

The possible contribution of gold RDE substrate to this Pd based catalyst's oxygen reduction activity should be discussed, as well. Although it is well known that gold catalysts are much more active toward ORR in alkaline media than in acidic media, it is exactly fact for Au nanoparticles at carbon or non-carbon based support, or at some other interactive supporting materials. As for polycrystalline gold it was referred that Au is relatively inert in the bulk polycrystalline state but exhibits good catalytic activity at the nanoscale [50,51]. To elucidate the role of the golden RDE we have also presented the polarization curve for ORR at polycrystalline gold RDE, at the same experimental conditions, Fig.S7 in Electronic supporting information. It can be seen that onset potential for Au electrode is 0.9 V vs RHE and half wave potential is ~0.8 V vs RHE. Thus the gold contribution to the overall oxygen reduction current density at the half wave potential of 0.90 V vs RHE for Pd based nanocatalyst at core-shell tungsten support can be neglected. The above mentioned data for onset and half wave potentials values at gold electrode are in good accordance to already published data in review paper from ACS Catalysis [50].

4. Conclusion

Tungsten based support was succesfully sinthesized and applied as a support for Pd nanoparticles. HRTEM analysis revealed core shell type structure of the support, the core made of W and shell from mixture of tungsten based oxide (WO_3) and carbide (WC). As for Pd nanoparticles onto this support, the homogenous distribution with average particle size of 2.5 nm was confirmed, even the cluster of single Pd atoms were detected by HRTEM. XPS analysis confirmed the presence W, WC and WO_3 species in the tungsten based support and Pd based ones in the Pd/W@WCWO$_3$ catalyst.

Determined very high electrochemically active surface area was in accordance to really small particle size previously detected by HRTEM. This fact gives the current catalyst great advantage in terms of high noble metal utilisation, in other words lower mass can be applied and spread owing to the extremely high surface area. Very high activity of the Pd/W@WCWO$_3$ catalyst, especially in alkaline soulutions was confirmed by electrochemical measurements. ORR activity expresed in terms of onset and half wave potential, as well as kinetic current density at 0.85 V vs RHE, and obtained values were comparable even to Pt based catalysts in the same electrolyte. Accelareted stability tests proved high stability and durability of the Pd/W@WCWO$_3$ catalyst, with neglectable activity changes before and after stability testing performed. It was explaned by high stability tungsten based support in the potential range of practical interest for low temperature fuel cells. High activity and stability of the catalyst make it promisssing as a cathode in low temperature fuel cells, especially having in mind about much higher price and much lower abbundance of Pt, compared to Pd.

Acknowledgements

This work was financially supported by Ministry of Education, Science and Technological Development of the Republic of Serbia under contract No. 172054.

The authors would like to acknowledge the COST MP1407 action for networking.

Electron microscopy characterization was performed at the National Center for Electron Microscopy at LBNL, Berkeley USA, supported by the Office of Science, Office of Basic Energy Sciences, of the U.S. Department of Energy under Contract No. DE-AC02-05CH11231.

Appendix A. Supplementary data

Supplementary data associated with this article can be found, in the online version, at http://dx.doi.org/10.1016/j.electacta.2017.07.066.

References

[1] U.A. Paulus, T.J. Schmidt, H.A. Gasteiger, R.J. Behm, Oxygen reduction on a high-surface area Pt/Vulcan carbon catalyst: A thin-film rotating ring-disk electrode study, Journal of Electroanalytical Chemistry 495 (2001) 134–145.

[2] K.J.J. Mayrhofer, D. Strmcnik, B.B. Blizanac, V. Stamenkovic, M. Arenz, N.M. Markovic, Measurement of oxygen reduction activities via the rotating disc electrode method: From Pt model surfaces to carbon-supported high surface area catalysts, Electrochimica Acta 53 (2008) 3181–3188.

[3] S. Zhang, Y. Shao, G. Yin, Y. Lin, Self-assembly of Pt nanoparticles on highly graphitized carbon nanotubes as an excellent oxygen-reduction catalyst, Applied Catalysis B: Environmental 102 (2011) 372–377.
[4] T. Kottakkat, A.K. Sahu, S.D. Bhat, P. Sethuraman, S. Parthasarathi, Catalytic activity of dendrimer encapsulated Pt nanoparticles anchored onto carbon towards oxygen reduction reaction in polymer electrolyte fuel cells, Applied Catalysis B: Environmental 110 (2011) 178–185.
[5] D. Sebastián, A.G. Ruíz, I. Suelves, R. Moliner, M.J. Lázaro, V. Baglio, A. Stassi, A.S. Aricò, Enhanced oxygen reduction activity and durability of Pt catalysts supported on carbon nanofibers, Applied Catalysis B: Environmental 115–116 (2012) 269–275.
[6] C.J. Zhong, J. Luo, P.N. Njoki, D. Mott, B. Wanjala, R. Loukrakpam, S. Lim, L. Wang, B. Fang, Z. Xu, Fuel cell technology: nano-engineered multimetallic catalysts, Energy Environ. Sci. 1 (2008) 454–466.
[7] N.R. Elezovic, V.R. Radmilovic, N.V. Krstajic, Platinum nanocatalysts on metal oxide based supports for low temperature fuel cell applications, RSC Advances 6 (2016) 6788–6801.
[8] T. Toda, H. Igarashi, H. Uchida, M. Watanabe, Enhancement of the Electroreduction of Oxygen on Pt Alloys with Fe, Ni, and Co, Journal of the Electrochemical Society 146 (1999) 3750–3756.
[9] C.A. Reiser, L. Bregoli, T.W. Patterson, S.Yi. Jung, J.D. Yang, M.L. Perry, T.D. Jarvi, A Reverse-Current Decay Mechanism for Fuel Cells, Electrochemical and Solid-State Letters 8 (2005) A273–A276.
[10] I. Takahashi, S.S. Kocha, Examination of the activity and durability of PEMFC catalysts in liquid electrolytes, Journal of Power Sources 195 (2010) 6312–6322.
[11] K. Hartl, M. Hanzlik, M. Arenz, IL-TEM investigations on the degradation mechanism of Pt/C electrocatalysts with different carbon supports, Energy Environ. Sci. 4 (2011) 234–238.
[12] S. Pylypenko, A. Borisevich, K.L. More, A.R. Corpuz, T. Holme, A.A. Dameron, T.S. Olson, H.N. Dinh, T. Gennette, R. O'Hayre, Nitrogen: unraveling the secret to stable carbon-supported Pt-alloy electrocatalysts, Energy Environ. Sci. 6 (2013) 2957–2964.
[13] X. Zhao, M. Yin, L. Ma, L. Liang, C. Liu, J. Liao, T. Luc, W. Xing, Recent advances in catalysts for direct methanol fuel cells, Energy Environ. Sci. 4 (2011) 2736–2753.
[14] A. Morozan, B. Jousselme, S. Palacin, Low-platinum and platinum-free catalysts for the oxygen reduction reaction at fuel cell cathode, Energy Environ. Sci. 4 (2011) 1238–1254.
[15] B. Wang, Recent development of non-platinum catalysts for oxygen reduction reaction, Journal of Power Sources 152 (2005) 1–15.
[16] G. Vijayaraghavan, K.J. Stevenson, Chemical Vapor Deposition of Nanocarbon-Supported Platinum and Palladium Catalysts for Oxygen Reduction, ECS Transactions 6 (2008) 43–50.
[17] K.K. Maniam, R. Chetty, Palladium Nanodendrites Deposited on Electrochemically Activated Carbon Based Support for Electrocatalytic Applications, ECS Transactions 61 (12) (2014) 11–20.
[18] L.M.R. Gavidia, G. García, D. Anaya, A. Querejeta, F. Alcaide, E. Pastor, Carbon-supported Pt-free catalysts with high specificity and activity toward the oxygen reduction reaction in acidic medium, Applied Catalysis B: Environmental 184 (2016) 12–19.
[19] C. Koenigsmann, S.S. Wong, One-dimensional noble metal electrocatalysts: a promising structural paradigm for direct methanol fuel cells, Energy Environ. Sci. 4 (2011) 1161–1176.
[20] R.G. González-Huerta, M.L. Luna-Martínez, O. Solorza-Feria, Electrochemical Characterization of Palladium Supported in Thermally Treated Carbon for Oxygen Reduction Reaction in Acid Media, ECS Transactions 20 (1) (2009) 267–274.
[21] L. Jiang, A. Hsu, D. Chu, R. Chen, Oxygen Reduction Reaction on Carbon Supported Pt and Pd in Alkaline Solutions, Journal of The Electrochemical Society 156 (3) (2009) B370–B376.
[22] L. Cheng, Z. Zhang, W. Niu, G. Xu, L. Zhu, Carbon-supported Pd nanocatalyst modified by non-metal phosphorus for the oxygen reduction reaction, Journal of Power Sources 182 (2008) 91–94.
[23] L. Xiao, L. Zhuang, Y. Liu, J. Lu, H.D. Abruna, Activating Pd by Morphology Tailoring for Oxygen Reduction, J. AM. CHEM. SOC 131 (2009) 602–608.
[24] M. Shao, Palladium-based electrocatalysts for hydrogen oxidation and oxygen reduction reactions, Journal of Power Sources 196 (2011) 2433–2444.
[25] M. Xia, Z. Y.Liu, S. Wei, K. Chen, L. Xiong, W. Li, J. Ding, Li-Jun Wan Hu, R. Lia, S.F. Alvia, Pd-induced Pt(IV) reduction to form Pd@Pt/CNT core@shell catalyst for a more complete oxygen reduction, J. Mater. Chem. A 1 (2013) 14443–14448.
[26] E. Antolini, Palladium in fuel cell catalysis, Energy Environ. Sci. 2 (2009) 915–931.
[27] R. Carrera-Cerritos, V. Baglio, A.S. Aricò, J. Ledesma-García, M.F. Sgroi, D. Pullini, A.J. Pruna, D.B. Mataix, R. Fuentes-Ramírez, L.G. Arriaga, Improved Pd electro-catalysis for oxygen reduction reaction in direct methanol fuel cell by reduced graphene oxide, Applied Catalysis B: Environmental 144 (2014) 554–560.
[28] Carmelo Lo Vecchio, Cinthia Alegre, David Sebastián, Alessandro Stassi, Antonino S. Aricò, Vincenzo Baglio, Investigation of Supported Pd-Based Electrocatalysts for the Oxygen Reduction Reaction: Performance, Durability and Methanol Tolerance, Materials 8 (12) (2015) 7997–8008.
[29] N.R. Elezovic, B.M. Babic, P. Ercius, V.R. Radmilovic, Lj.M. Vracar, N.V. Krstajic, Synthesis and characterization Pt nanocatalysts on tungsten based supports for oxygen reduction reaction, Applied Catalysis B: Environmental 125 (2012) 390–397.
[30] B. Han, C.E. Carlton, A. Kongkanand, R.S. Kukreja, B.R. Theobald, L. Gan, R.l O'Malley, P. Strasser, F.T. Wagner, Y. Shao-Horn, Record activity and stability of dealloyed bimetallic catalysts for proton exchange membrane fuel cells, Energy Environ. Sci. 8 (2015) 258–266.
[31] N.V. Alov, Determination of the States of Oxidation of Metals in Thin Oxide Films by X-Ray Photoelectron Spectroscopy, Journal of Analytical Chemistry 60 (2005) 431–435.
[32] Alireza Babaei, San Ping Jiang, Jian Li, Electrocatalytic Promotion of Palladium Nanoparticles on Hydrogen Oxidation on Ni/GDC Anodes of SOFCs via Spillover, Journal of The Electrochemical Society 156 (9) (2009) B1022–B1029.
[33] H. Xu, L.-X. Ding, Ch.-L. Liang, Y.-X. Tong, G.-R. Li, High-performance polypyrrole functionalized PtPd electrocatalysts based on PtPd/PPy/PtPd three-layered nanotube arrays for the electrooxidation of small organic molecules, NPG Asia Materials 5 (2013) e69.
[34] A. Katrib, F. Hemming, P. Wehrer, L. Hilaire, G. Maire, The multi-surface structure and catalytic properties of partially reduced WO3, WO2 and WC + O2 or W + O2 as characterized by XPS, Journal of Electron Spectroscopy and Related Phenomena 76 (1995) 195–200.
[35] F.Y. Xie, L. Gong, X. Liu, Y.T. Tao, W.H. Zhang, S.H. Chen, H. Meng, J.J. Chen, XPS studies on surface reduction of tungsten oxide nanowire film by Ar+ bombardment, Journal of Electron Spectroscopy and Related Phenomena 185 (2012) 112–118.
[36] C.B. Rodella, D.H. Barrett, S.F. Moya, S.J.A. Figueroa, M.T.B. Pimenta, A.A.S. Curvelo, V. Teixeira da Silva, Physical and chemical studies of tungsten carbide catalysts: effects of Ni promotion and sulphonated carbon, RSC Advances 5 (2015) 23874–23885.
[37] L. Fan, Q. Ta, M. Li, L. Liao, D. Chen, Y. Chen, Determination of the Real Surface Area of Palladium Electrode, Chinese Journal of Chemical Physics 23 (2010) 543–548.
[38] D.A.J. Rand, R.J. Woods, The nature of adsorbed oxygen on rhodium, palladium and gold electrodes, J. Electroanal. Chem. 31 (1971) 29–38.
[39] A.N. Correia, L.H. Mascaro, S.A.S. Machado, L.A. Avaca, Active surface area determination of Pd-Si alloys by H-adsorption, Electrochim. Acta 42 (1997) 493–495.
[40] Lj.M. Vracar, D.B. Sepa, A. Damjanovic, Palladium Electrode in Oxygen-Saturated Aqueous Solutions Potential Dependent Adsorption of Oxygen Containing Species and Their Effect on Oxygen Reduction, J. Electrochem. Soc. 136 (1989) 1973–1977.
[41] H.A. Gasteiger, S.S. Kocha, B. Sompalli, F.T. Wagner, Activity benchmarks and requirements for Pt, Pt-alloy, and non-Pt oxygen reduction catalysts for PEMFCs, Applied Catalysis B: Environmental 56 (2005) 9–35.
[42] Y. Holade, R.G. da Silva, K. Servat, T.W. Napporn, C. Canaff, A.R. de Andrade, K.B. Kokoh, Facile synthesis of highly active and durable PdM/C (M = Fe, Mn) nanocatalysts for the oxygen reduction reaction in an alkaline medium, J. Mater. Chem. A 4 (2016) 8337–8349.
[43] J.R. Varcoe, P. Atanassov, D.R. Dekel, A.M. Herring, M.A. Hickner, P.A. Kohl, A.R. Kucernak, W.E. Mustain, K. Nijmeijer, K. Scott, T. Xu, L. Zhuang, Anion-exchange membranes in electrochemical energy systems, Energy Environ. Sci. 7 (2014) 3135–3191.
[44] M.C. Weidman, D.V. Esposito, I.J. Hsu, J.G. Chen, Electrochemical Stability of Tungsten and Tungsten Monocarbide (WC) Over Wide pH and Potential Ranges, Journal of The Electrochemical Society 157 (12) (2010) F179–F188.
[45] M.B. Zellner, J.G. Chen, Surface science and electrochemical studies of WC and W_2C PVD films as potential electrocatalysts, Catalysis Today 99 (2005) 299–307.
[46] D.A.J. Rand, R. Woods, A Study of the Dissolution of Platinum Pallladium, rhodium and Gold Electrodes in 1 M Sulfuric Acid by Cyclic Voltammetry, J. Electroanal. Chem. 35 (1972) 209–218.
[47] S. Stolbov, M.A. Ortigoza, Rational Design of Competitive Electrocatalysts for Hydrogen Fuel Cells, J. Phys. Chem. Lett. 3 (2012) 463–467.
[48] N.R. Elezovic, B.M. Babic, Lj. Gajic-Krstajic, P. Ercius, V.R. Radmilovic, N.V. Krstajic, Lj.M. Vracar, Pt supported on nano-tungsten carbide as a beneficial catalyst for the oxygen reduction reaction in alkaline solution, Electrochimica Acta 69 (2012) 239–246.
[49] P. Quaino, N.B. Luque, R. Nazmutdinov, E. Santos, and Wolfgang Schmickler Why is Gold such a Good Catalyst for Oxygen Reduction in Alkaline Media, Angewandte Chemie International Edition 51 (2012) 12997–13000.
[50] X. Ge, A. Sumboja, D. Wuu, T. An, B. Li, F.W. Thomas Goh, T.S. Andy Hor, Y. Zong, Z. Liu, Oxygen Reduction in Alkaline Media: From Mechanisms to Recent Advances of Catalysts, ACS Catalysis 5 (2015) 4643–4667.
[51] S. Xu, P. Wu, Facile and green synthesis of a surfactant-free Au clusters/reduced graphene oxide composite as an efficient electrocatalyst for the oxygen reduction reaction, J. Mater. Chem. A 2 (2014) 13682–13690.